# CHAPTER IV
# RESULTS AND DISCUSSION

## 4.1 Characterization of adsorbents

### 4.1.1 BET surface area analysis

The BET surface area ($S_{BET}$), micropore volume ($V_{DR}$, using DUBININ-RADUSHKEVICH or DR method), total pore volume, and average pore diameter were obtained by BET surface analyzer using at -196°C using liquid nitrogen as mentioned in Chapter 3. The results of commercial available activated carbons (coconut-, palm-, and bituminous coal-based activated carbon) and as coconut-based activated carbon (activated by $K_2CO_3$) process are shown in Table 4.1.

**Table 4.1** Physical BET surface properties of studied activated carbons

| Activated carbon | BET surface area ($m^2/g$) | $V_{DR}$ (cc/g) | Total pore volume (cc/g) | DR micropore (Å) | Average pore diameter (Å) |
|---|---|---|---|---|---|
| A (IN 1100) | 918.6 | 0.49 | 0.50 | 16.14 | 21.89 |
| B (IN 1067) | 839.2 | 0.48 | 0.58 | 24.74 | 27.47 |
| C (IN 1100) | 801.9 | 0.43 | 0.44 | 17.03 | 22.10 |
| D (IN 937) | 776.6 | 0.42 | 0.44 | 22.52 | 22.89 |
| E (IN 1035) | 775.0 | 0.42 | 0.45 | 23.04 | 23.39 |
| F (IN 879) | 774.7 | 0.41 | 0.44 | 22.25 | 22.59 |
| G (IN 987) | 774.4 | 0.41 | 0.44 | 22.15 | 22.92 |
| Co-$K_2CO_3$/1h | 197.9 | 0.13 | 0.14 | 25.24 | 29.70 |
| Co-$K_2CO_3$/2h | 211.3 | 0.14 | 0.16 | 22.51 | 27.82 |
| Co-$K_2CO_3$/3h | 114.9 | 0.08 | 0.09 | 29.65 | 31.61 |

The commercial coconut-based activated carbon; A (IN 1100) has the highest BET surface area, micropore volume, and total pore volume following by B

(IN 1067), C (IN 1100), D (IN 937), E (IN 1035), F (IN 879), G (IN 987), Co-$K_2CO_3$/2h, Co-$K_2CO_3$/1h, and Co-$K_2CO_3$/3h, respectively. On the contrary, Co-$K_2CO_3$ has the larger pore diameter than commercial activated carbons. It is interesting to note that the activated carbons in this study have their average pore diameter greater than 20 Å.

The differences in the BET surface area, pore volume and pore size of activated carbons are due to the source of raw materials and also the method of activation; the commercial activated carbons are produced by steam activation process while coconut-base activated carbons produced in a laboratory was activated by $K_2CO_3$.

### 4.1.2 Field Emission Scanning Electron Microscope (FE-SEM)

Figure 4.1-4.12 show surface morphology of the surface of raw coconut shell and activated carbons at 2,500 and 5,000 magnifications. The surfaces of the coconut shells in Figure 4.1 were heterogeneous and rough. The majority average pore size diameter of the commercial activated carbons (Figure 4.2-4.8) was mesopores since the pores were developed by carbonization and steam activation process. These results were confirmed by BET surface area analyzer as shown in Table 4.1 with the higher the surface area of activated carbon, the higher amount of the micropores. Although, the majority average pore size diameters of commercial activated carbons are mesopores but at these magnifications, only the overall surface and macropores of the activated carbons can be observed.

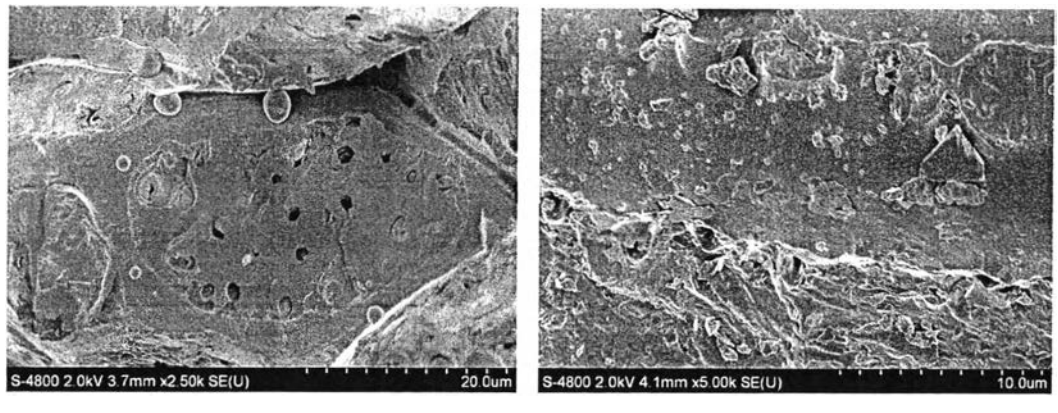


**Figure 4.1** FE-SEM micrographs of raw coconut shell.

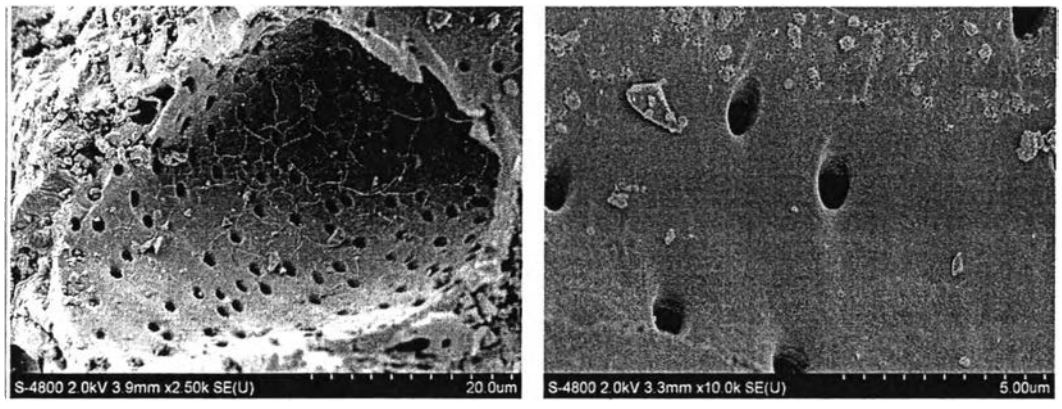


**Figure 4.2** FE-SEM images of coconut-based activated carbon (IN-1100).

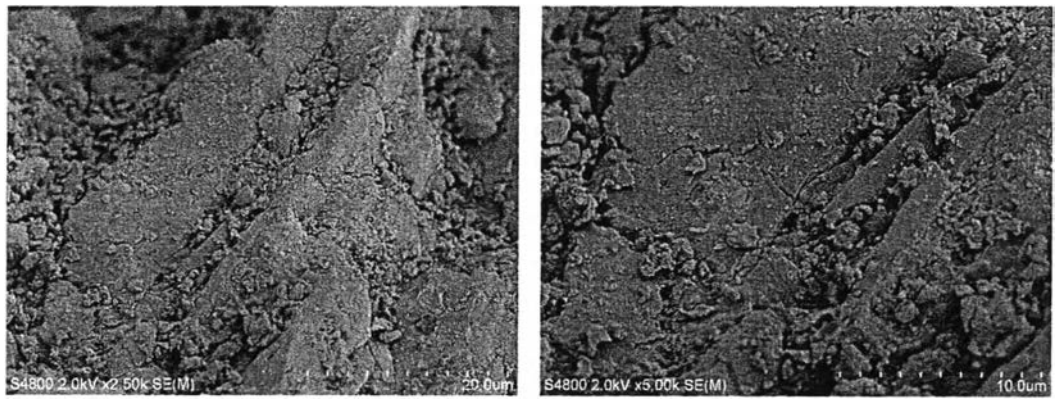


**Figure 4.3** FE-SEM images of bituminous coal-based activated carbon (IN-1067).

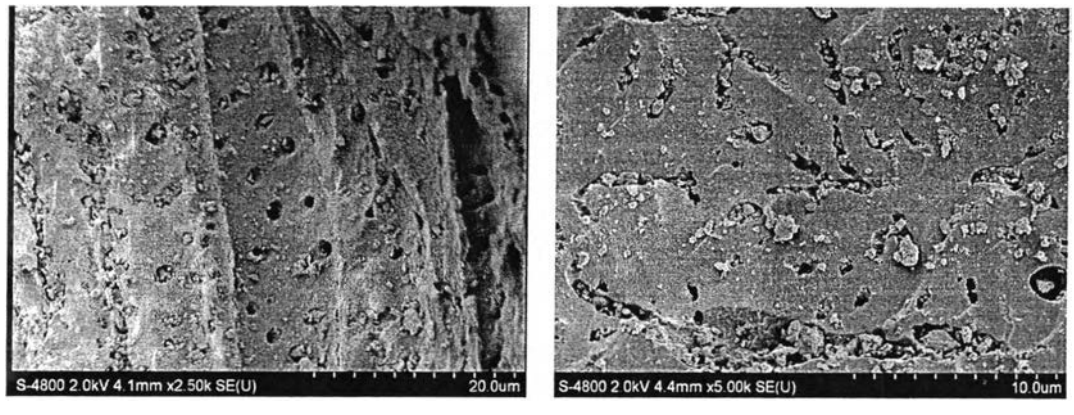


**Figure 4.4** FE-SEM images of palm-based activated carbon (IN-1100).

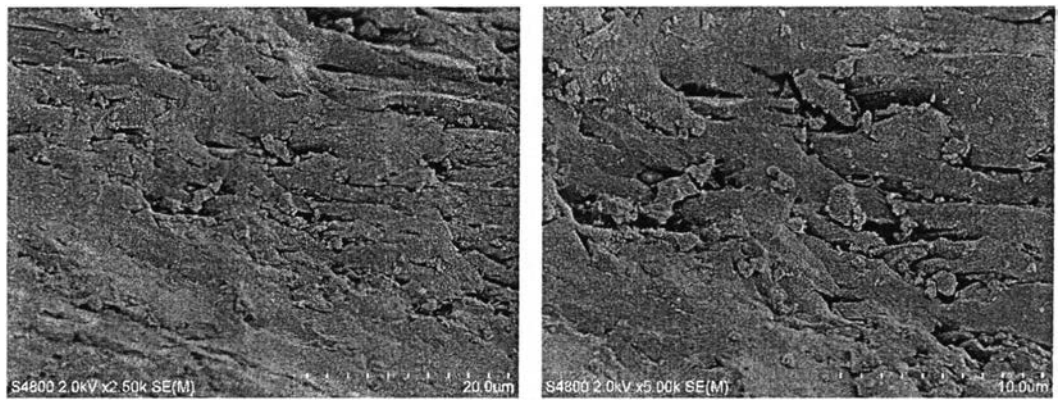


**Figure 4.5** FE-SEM images of bituminous coal-based activated carbon (IN-937).

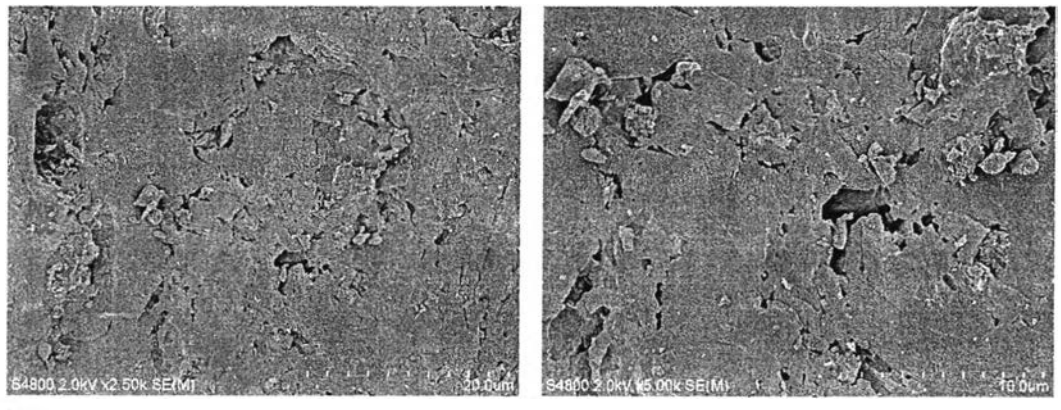


**Figure 4.6** FE-SEM images of bituminous coal-based activated carbon (IN-1035).

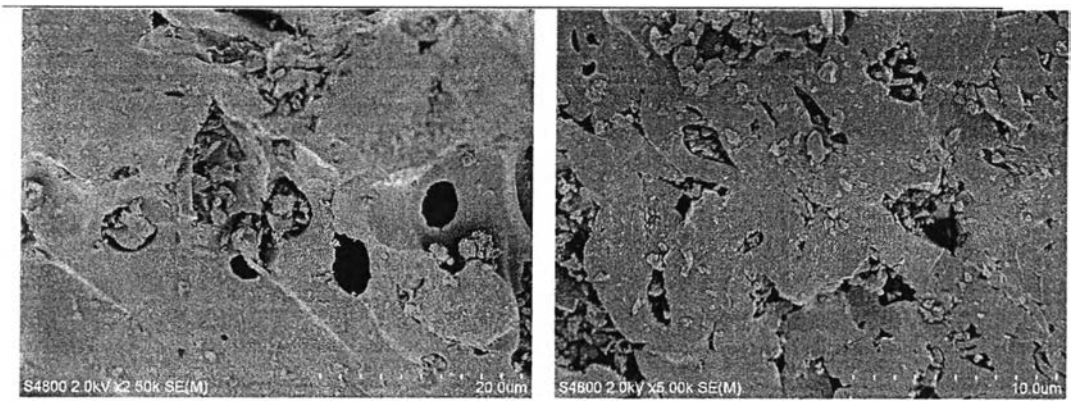


**Figure 4.7** FE-SEM images of bituminous coal-based activated carbon (IN-879).

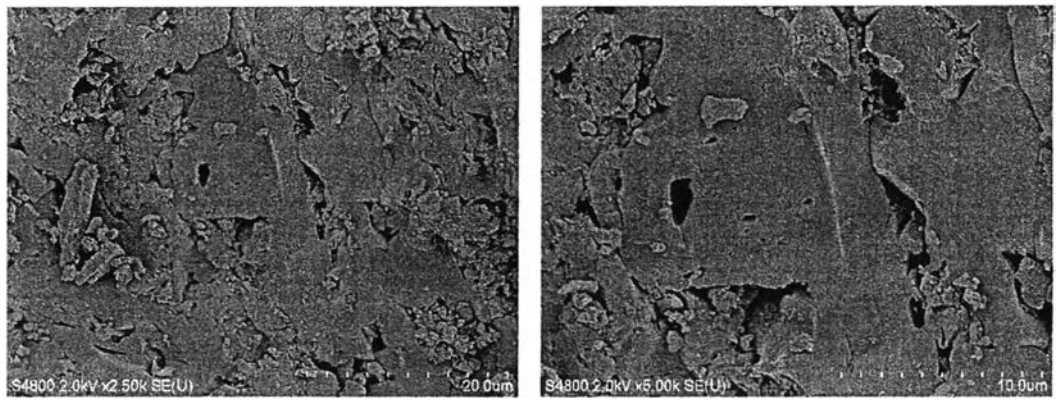


**Figure 4.8** FE-SEM images of bituminous coal-based activated carbon (IN-987).

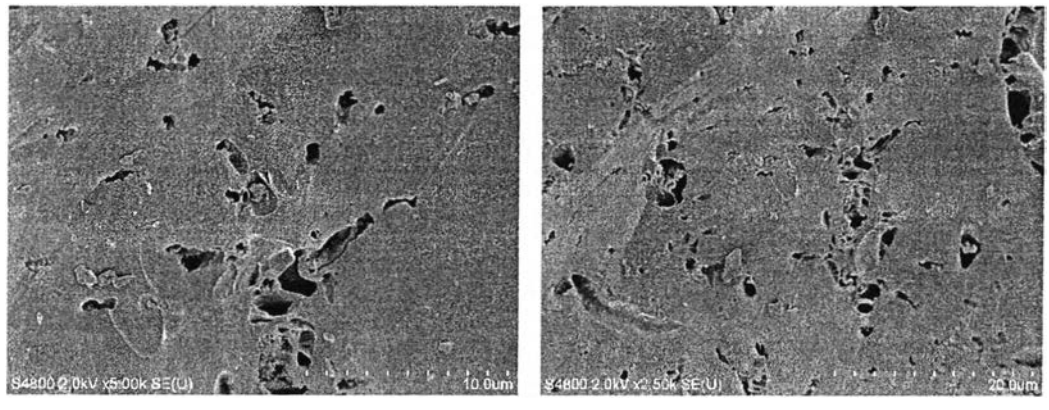


**Figure 4.9** FE-SEM images of coconut-based char at 400 °C and 60 min.

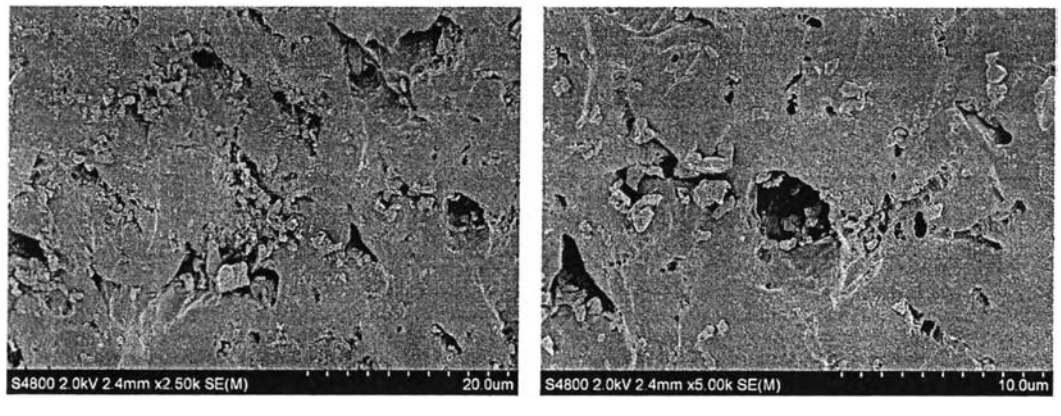


**Figure 4.10** FE-SEM images of coconut-based activated carbon with $K_2CO_3$/1 h.

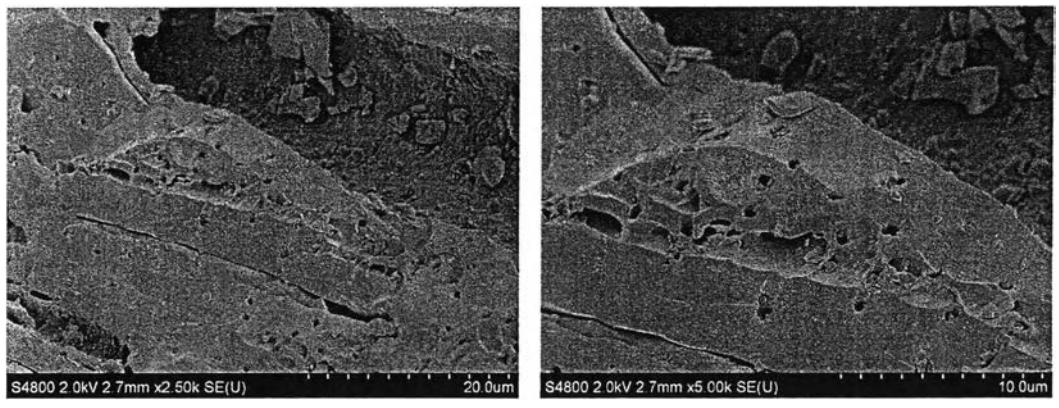


**Figure 4.11** FE-SEM images of coconut-based activated carbon with $K_2CO_3$/2 h.

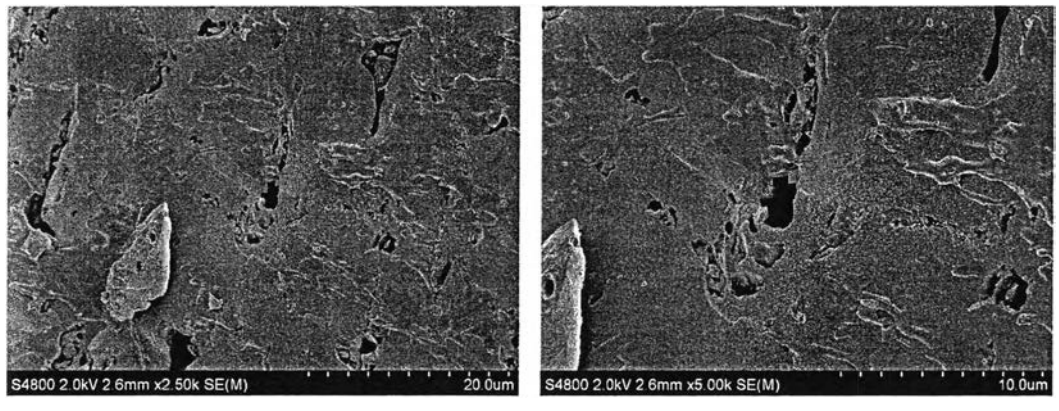


**Figure 4.12** FE-SEM images of coconut-based activated carbon with $K_2CO_3$/3 h.

## 4.2 Methane Adsorption by Activated Carbons

Figure 4.13-4.16 are the plots showing the relation between the amount of methane adsorption at 1,000 psia and 40°C as a function of BET surface area, micropore volume, total pore volume, and DR pore diameter, respectively. It can be observed that greater amount of methane adsorption was commercial activated carbon which occurred at a high BET surface area, micropore volume, and total pore volume. While, coconut-based activated carbon activated by $K_2CO_3$ presents the high pore diameter of activated carbon due to less micropore volume and BET surface area. A (IN 1100) was the highest methane adsorption due to the highest BET surface area and micropore volume. This result was corresponding to the physical properties of activated carbons in Table 4.1.

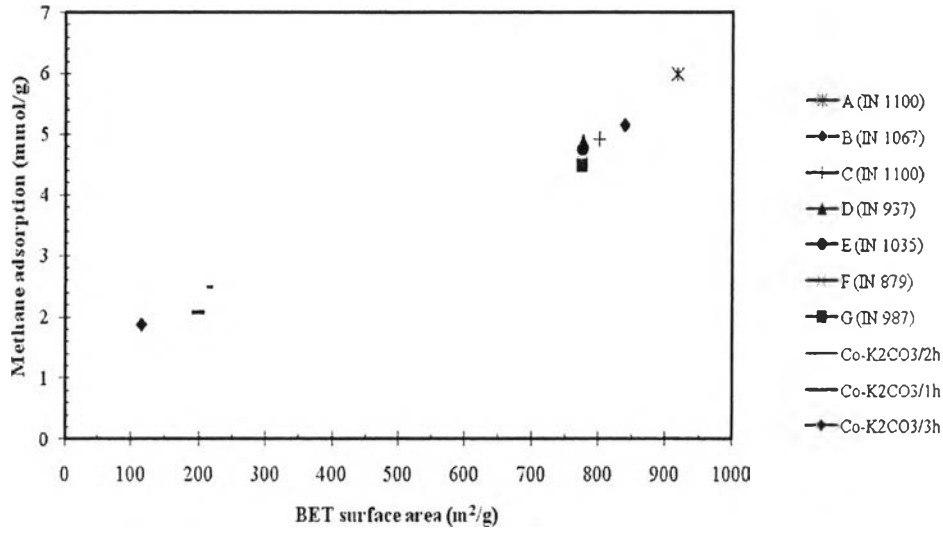


**Figure 4.13** Methane adsorption (mmol/g) at 1,000 psia and 40 °C as a function of BET surface area ($m^2/g$).

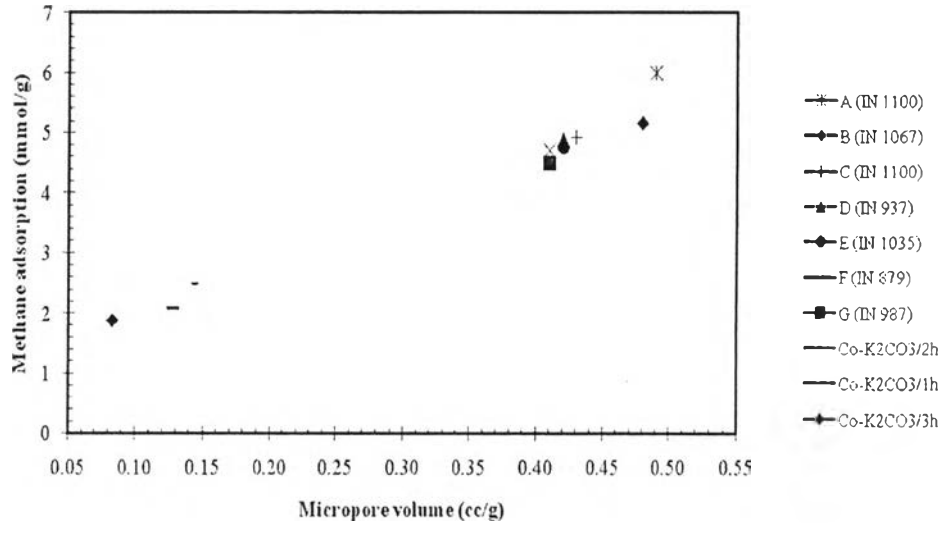


**Figure 4.14** Methane adsorption (mmol/g) at 1,000 psia and 40 °C as a function of micropore volume (cc/g).

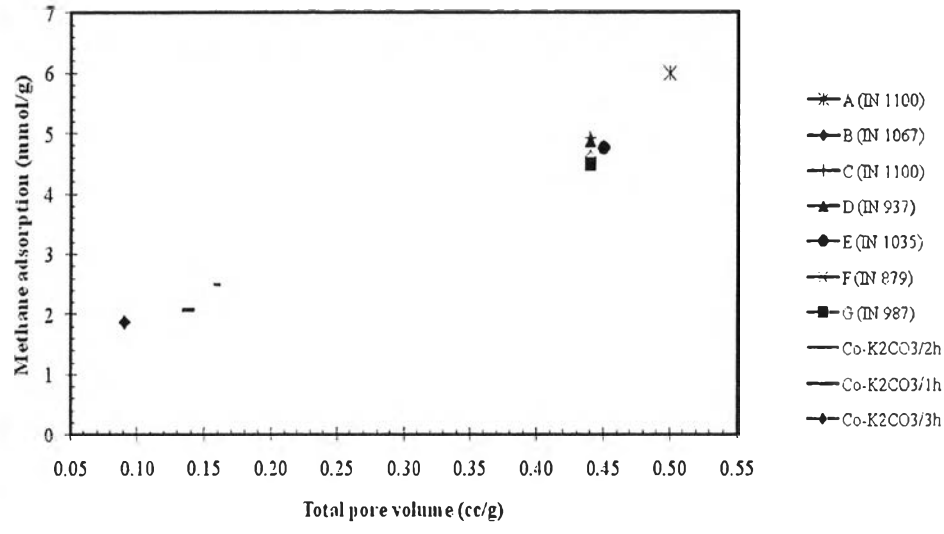


**Figure 4.15** Methane adsorption (mmol/g) at 1,000 psia and 40 °C as a function of total pore volume (cc/g).

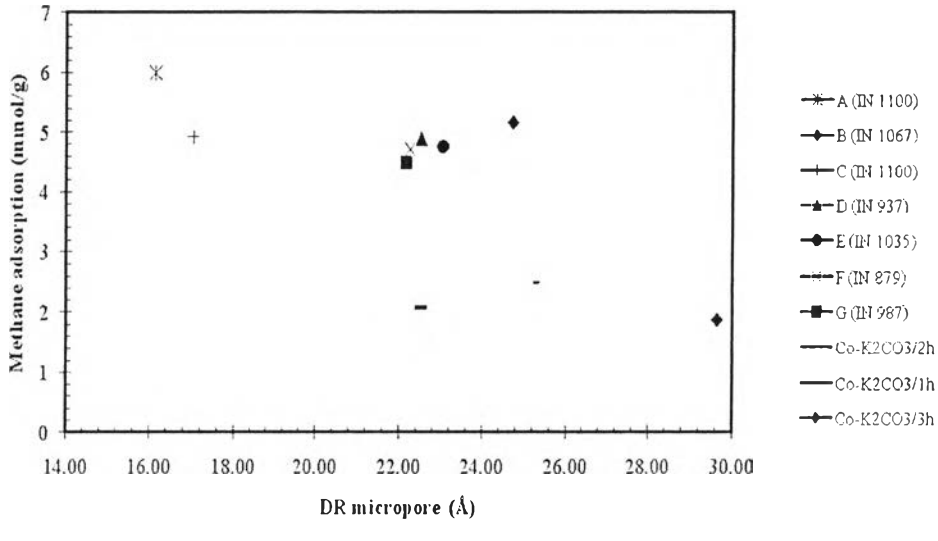


**Figure 4.16** Methane adsorption (mmol/g) at 1,000 psia and 40 °C as a function of DR micropore (Å).

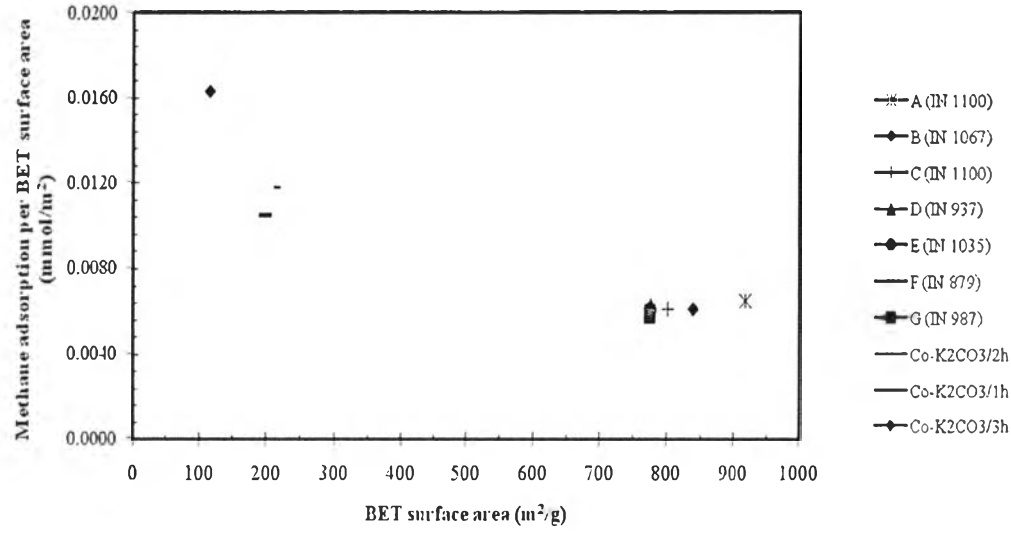


**Figure 4.17** Methane adsorption per BET surface area (mmol/$m^2$) at 1,000 psia and 40 °C as a function of BET surface area ($m^2$/g).

Figure 4.17 presents the amount of methane adsorption per BET surface area (mmol/$m^2$) at 1,000 psia as a function of BET surface area. Methane adsorption per BET surface area of commercial activated carbon was lower than coconut-based activated carbon activated by $K_2CO_3$ because of its higher BET surface area. Co-$K_2CO_3$/3h has the highest methane adsorption capacity per BET surface area due to the lowest BET surface area.

Figure 4.18-4.20 show methane adsorption on activated carbons; A (IN 1100), B (IN 1067), C (IN 1100), D (IN 937), E (IN 1035), F (IN 879), G (IN 987), Co-$K_2CO_3$/1h, Co-$K_2CO_3$/2h, and Co-$K_2CO_3$/3h at 35, 40, and 45 °C with the pressure in the range of 0 to 1,000 psia. The methane adsorption isotherm was plotted between the amount of methane adsorbed (mmol) per gram of adsorbent (activated carbon) and equilibrium pressure of methane (psia).

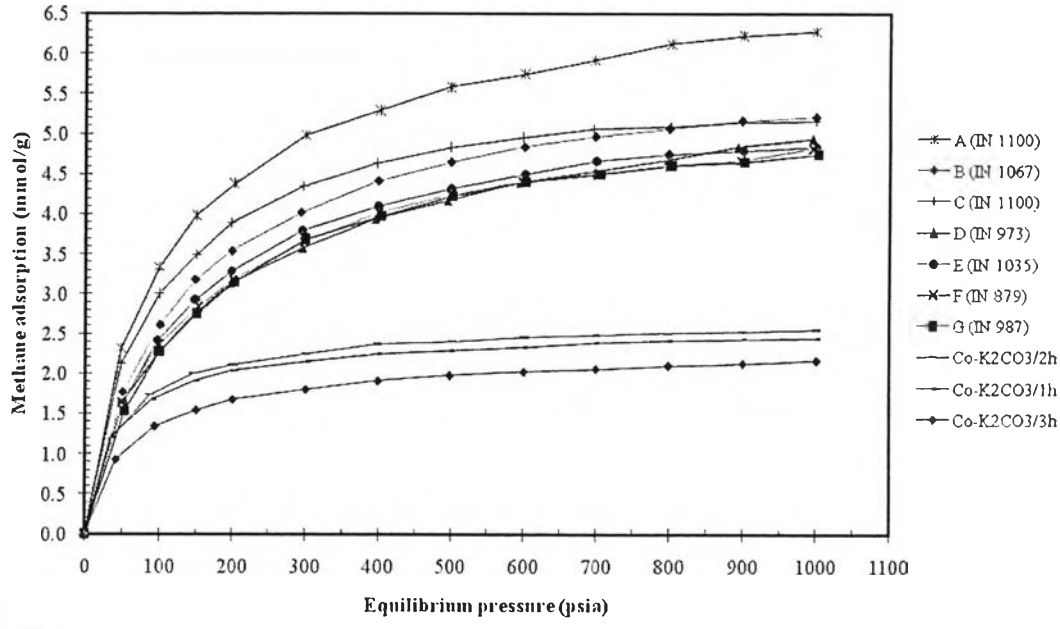


**Figure 4.18** Methane adsorption on activated carbons at 35°C.

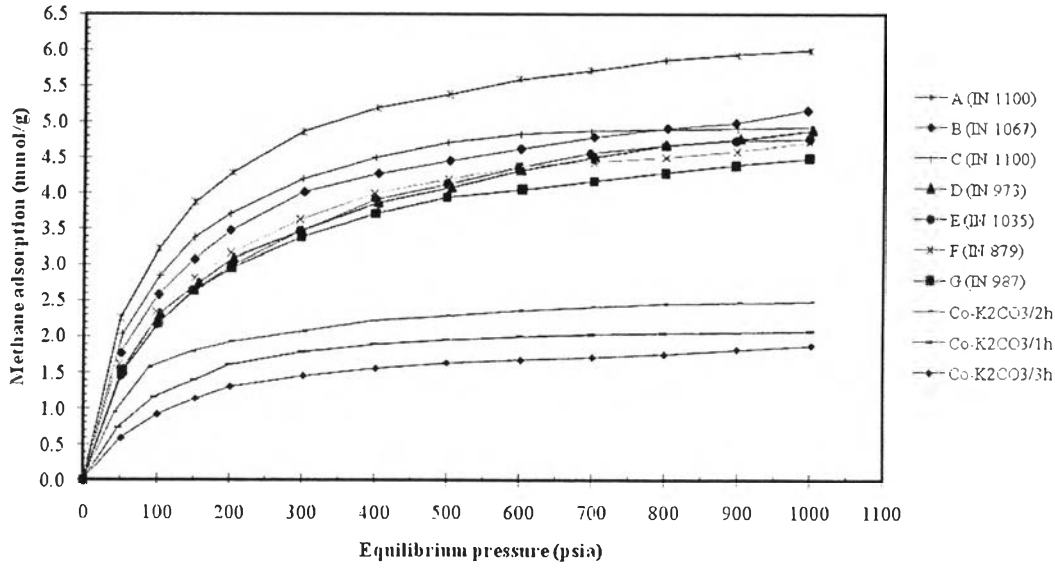


**Figure 4.19** Methane adsorption on activated carbons at 40°C.

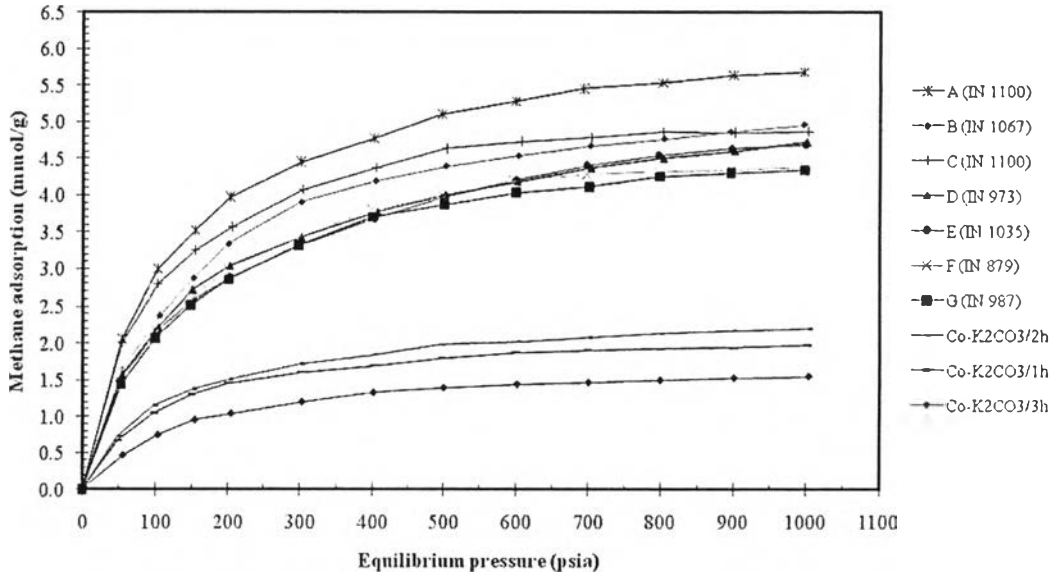


**Figure 4.20** Methane adsorption on activated carbons at 45°C.

The pore size of activated carbon is also an important parameter. The chemicals and technique that used in this study strongly affected the final pore size. Furthermore, the optimum pore size for methane storage is approximately 11.4 Å (Matranga *et al.*, 1992). As a result, the increased in the methane adsorption capacity probably mainly because of the increased in the surface area.

Iodine number is a significant characteristic of activated carbon. The iodine number gives a measure of micropore volume of activated carbon and it approximates to total internal surface of the activated carbon (Yusufu *et al.*, 2012). Thus, higher iodine values (mg/g) led to higher amount of micropore volume of commercial activated carbons which result in the higher amount of methane adsorbed than that the commercial activated carbons with lower iodine values. However, methane adsorption is not depending only on iodine number, but also depending on the pore size diameter and BET surface of the commercial activated carbons.

The result showed that the amount of methane adsorption increases with an increase in the pressure. The methane adsorption capacity (mmol) per gram of activated carbon of commercial activated carbon was greater than coconut-based activated carbon produced by $K_2CO_3$ activation process. The commercial coconut-based activated carbon; A (IN 1100) can adsorb the highest amount of methane,

following by B (IN 1067), C (IN 1100), D (IN 937), E (IN 1035), F (IN 879), G (IN 987), Co-$K_2CO_3$/2h, Co-$K_2CO_3$/1h, and Co-$K_2CO_3$/3h.

Therefore, activated carbon adsorbed high amount of methane when it had a high BET surface area (great pore developed), micropore volume, total pore volume, and the pore size of activated carbon was nearly 11.4 Å.

By increasing the activation time of Co-$K_2CO_3$ up to 120 min, methane adsorption was increased but at activation time 180 min, methane adsorption was decreased. The decreased was due to the presence in higher amount of mesopores and a much lower micropore volume which does not present the suitable pore structure required for good methane adsorption capacity (Lozano-Castelló *et al.*, 2002). This is corresponding to the physical properties in Table 4.1.

**Table 4.2** The capacity of methane adsorption (mmol/g) at 1,000 psia and different temperature

| Activated carbon | The amount of Methane Adsorption (mmol/g) at 1,000 psia | | |
|---|---|---|---|
| | 35 °C | 40 °C | 45 °C |
| A (IN1100) | 6.282 | 5.992 | 5.682 |
| B (IN 1067) | 5.212 | 5.157 | 4.956 |
| C (IN 1100) | 5.161 | 4.918 | 4.868 |
| D (IN 937) | 4.938 | 4.881 | 4.725 |
| E (IN 1035) | 4.841 | 4.758 | 4.689 |
| F (IN 879) | 4.816 | 4.710 | 4.390 |
| G (IN 987) | 4.743 | 4.488 | 4.342 |
| Co-$K_2CO_3$/1h | 2.443 | 2.078 | 1.972 |
| Co-$K_2CO_3$/2h | 2.552 | 2.490 | 2.197 |
| Co-$K_2CO_3$/3h | 2.163 | 1.916 | 1.445 |

In addition, at low temperature the capacity of methane adsorption was higher than methane adsorption at high temperature as illustrated in Table 4.2. This is mainly due to the physisorption behaviors on the surface of activated carbons.

However, the methane adsorption at high pressure was increased slightly due to the saturation of adsorbent (activated carbon) (Delavar *et al.*, 2010).

The amount of methane adsorption per BET surface area (mmol/$m^2$) of activated carbons as a function of equilibrium pressure (psia) at temperature of 35, 40, and 45°C were presented in Figure 4.21-4.23 and Table 4.3.

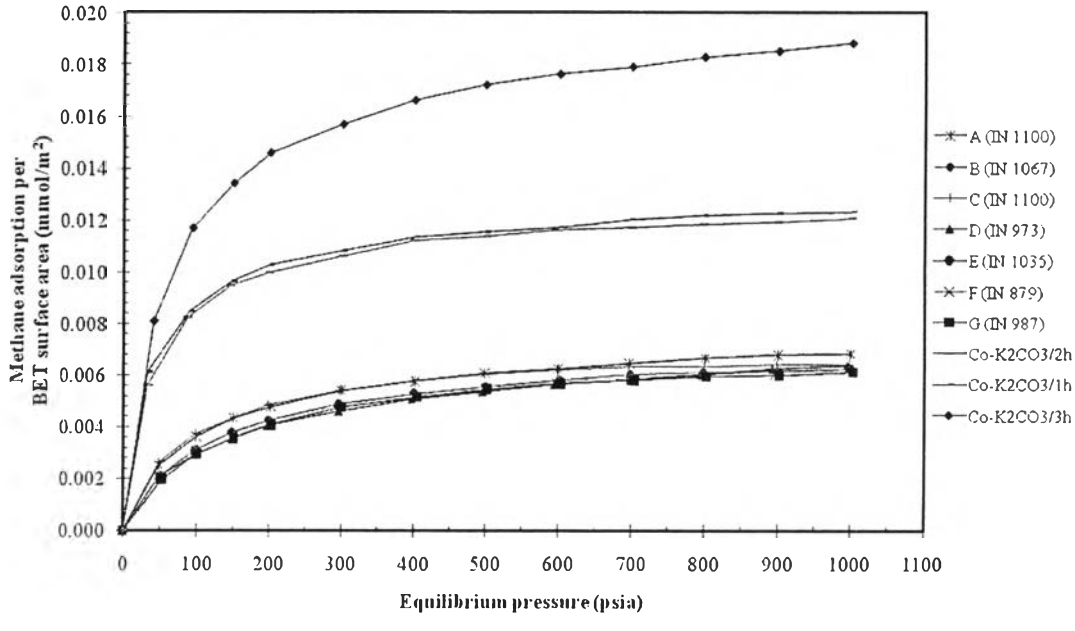


**Figure 4.21** Methane adsorption per BET surface (mmol/$m^2$) of activated carbons as a function of equilibrium pressure (psia) at 35°C.

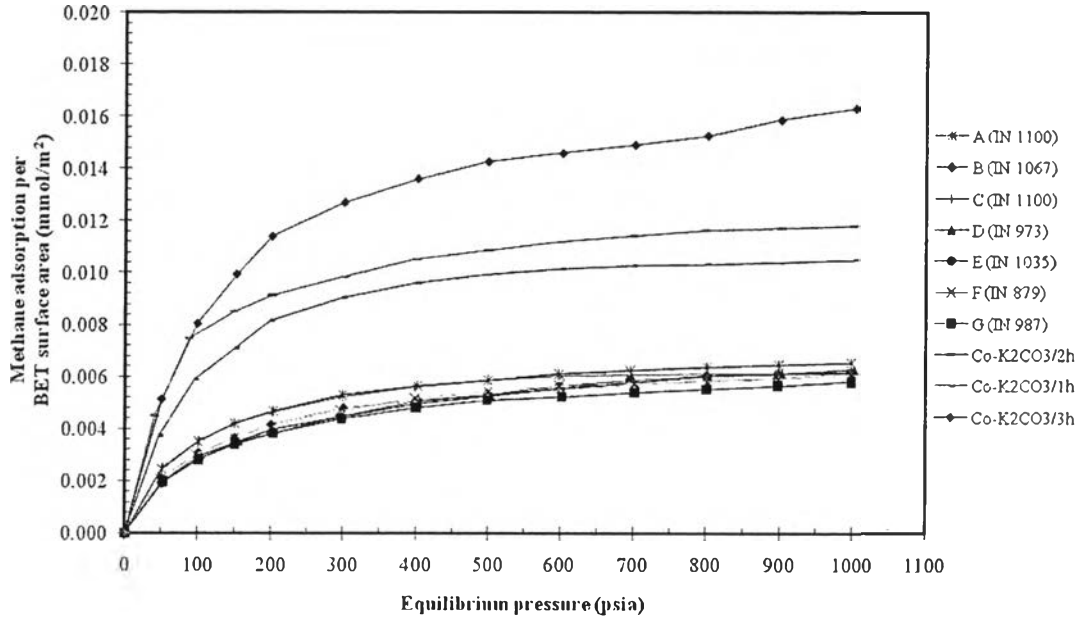


**Figure 4.22** Methane adsorption per BET surface (mmol/m$^2$) of activated carbons as a function of equilibrium pressure (psia) at 40°C.

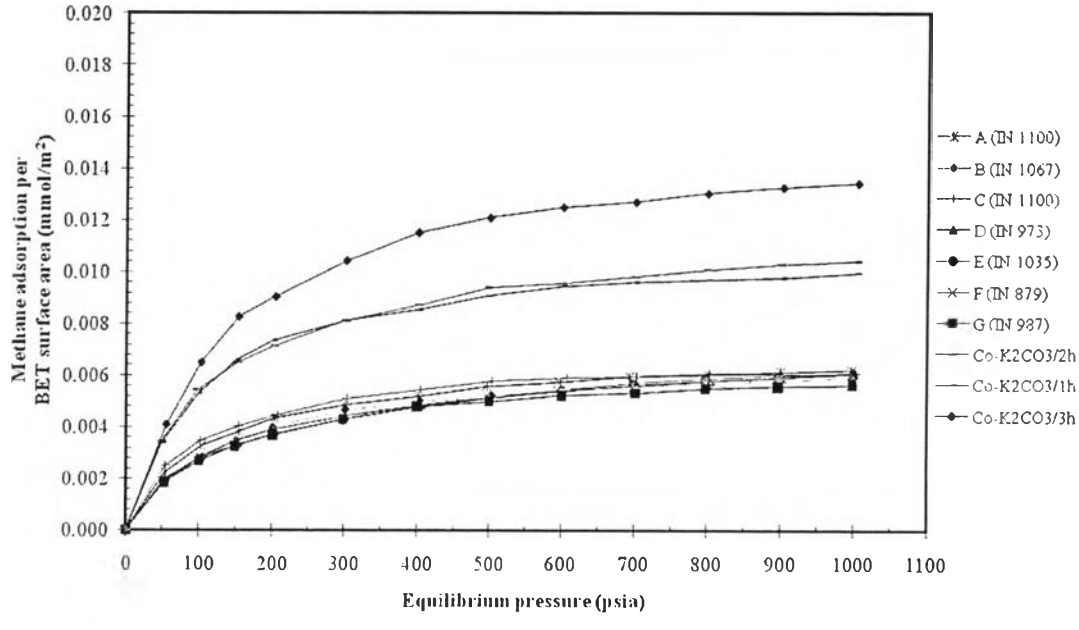


**Figure 4.23** Methane adsorption per BET surface (mmol/m$^2$) of activated carbons as a function of equilibrium pressure (psia) at 45°C.

The result indicated that all of the activated carbons had not the same capacity of methane adsorption per BET surface area; implied that the amount of methane adsorption was not only depend on the BET surface area but also micropore volume, and pore size diameter.

**Table 4.3** The capacity of methane adsorption per BET surface area ($mmol/m^2$) at 1,000 psia and different temperature

| Activated carbon | The amount of Methane Adsorption per BET surface area ($mmol/m^2$) at 1,000 psia | | |
|---|---|---|---|
| | 35 °C | 40 °C | 45 °C |
| A (IN1100) | 0.0068 | 0.0065 | 0.0062 |
| B (IN 1067) | 0.0062 | 0.0061 | 0.0059 |
| C (IN 1100) | 0.0064 | 0.0061 | 0.0061 |
| D (IN 937) | 0.0063 | 0.0063 | 0.0061 |
| E (IN 1035) | 0.0062 | 0.0061 | 0.0060 |
| F (IN 879) | 0.0062 | 0.0061 | 0.0057 |
| G (IN 987) | 0.0061 | 0.0058 | 0.0056 |
| Co-$K_2CO_3$/1h | 0.0123 | 0.0105 | 0.0010 |
| Co-$K_2CO_3$/2h | 0.0121 | 0.0118 | 0.0104 |
| Co-$K_2CO_3$/3h | 0.0188 | 0.0163 | 0.0134 |

Although the amount of methane adsorption (mmol) per gram of commercial activated carbon was higher than coconut-based activated carbon produced by $K_2CO_3$ activation but methane adsorption per BET surface area ($mmol/m^2$) of commercial activated carbon was lower than coconut-based activated carbon produced by $K_2CO_3$ activation. This was because of its higher BET surface area, micropore volume, less pore diameter of commercial activated carbon. While, Co-$K_2CO_3$/3h has the highest methane adsorption capacity per BET surface area due to the lowest BET surface area, micropore volume, and the highest pore diameter.

Furthermore, at low temperature the capacity of methane adsorption per BET surface area was higher than that of methane adsorption per BET surface area at high temperature.

The capacity of methane adsorption per BET surface area (mmol/$m^2$) of activated carbons at temperature of 35°C compared with previous work (Kumpoomee, 2012) was presented in Figure 4.24.

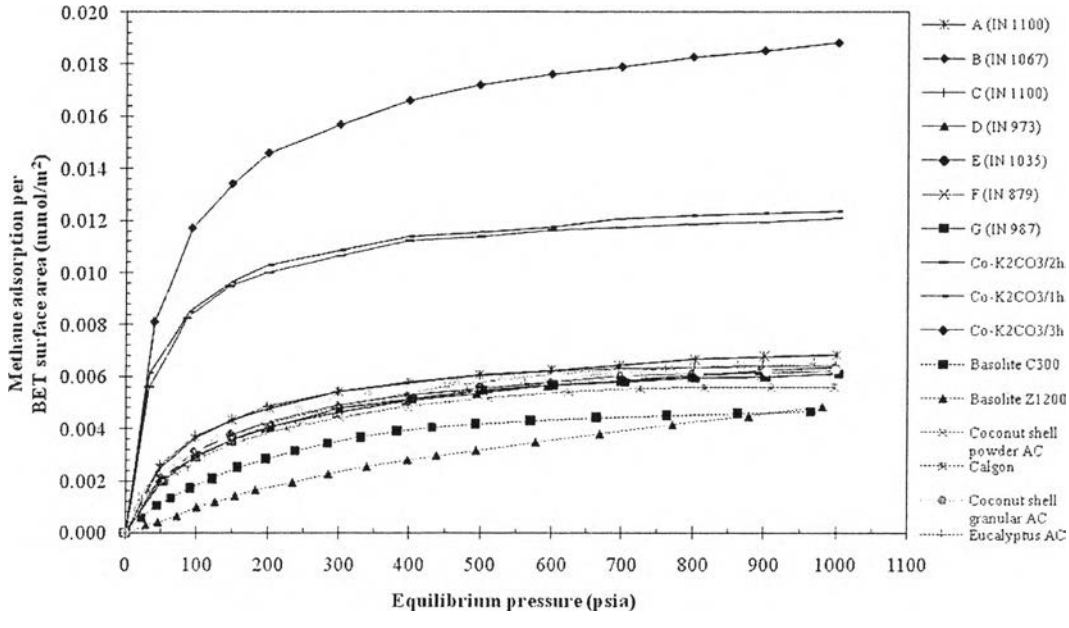


**Figure 4.24** Methane adsorption per BET surface (mmol/$m^2$) of activated carbons as a function of equilibrium pressure (psia) at 35°C compared with previous work (Kumpoomee, 2012).

When compare the amount of methane adsorbed per the same unit of BET surface area (mmol/$m^2$) on all adsorbents, it can imply that coconut-based activated carbon activated by $K_2CO_3$ which has less BET surface area presented the high capacity of methane adsorption per 1 $m^2$ of BET surface area than the others. It may be the $K_2CO_3$ activation process is not suitable for methane adsorption due to it gives low BET surface area; therefore it should be develop the activation process to increase the surface area per gram. The A (IN 1100) was the highest methane adsorption per BET surface area.

Basolite C300 and Basolite Z1200 which have a very high BET surface and micropore volume area were presented the lowest methane adsorption capacity per the same unit of BET surface area (mmol/$m^2$). It may be due to the methane cannot enter to their micropore, result in less methane adsorption on Basolite C300 and Basolite Z1200. Basolite C300 was the lowest methane adsorption per 1 $m^2$ of BET surface area.

In addition, commercial activated carbon, coconut shell powder activated carbon, calgon, coconut shell granular activated carbon, and eucalyptus activated carbon showed the same adsorption capacity per the same unit of BET surface area because of the BET surface area of commercial-, coconut shell powder-, calgon, coconut shell granular-, and eucalyptus activated carbon were very close.

## 4.3 Production of activated carbons

### 4.3.1 Carbonization process

Carbonization of coconut shell was carried out under constant nitrogen flow rate (150 ml/min) and heated up with the rate of 10 °C/min to a different temperatures and different times. The results are shown in Table 4.4 and Figures 4.25-4.26.

**Table 4.4** Characteristics of carbonized coconut shell at different conditions

| Sample | $N_2$ flow rate (ml/min) | Heating rate (°C/min) | Temperature (°C) | Time (min) | Burn-off (%) | Yield (%) |
|---|---|---|---|---|---|---|
| 1 | 150 | 10 | 400 | 30 | 69.8 | 30.2 |
| 2 | | | | 60 | 70.8 | 29.2 |
| 3 | | | | 90 | 71.3 | 28.7 |
| 4 | | | | 120 | 71.7 | 28.3 |
| 5 | | | | 150 | 72.2 | 27.8 |
| 6 | | | 500 | 60 | 72.5 | 27.5 |
| 7 | | | 600 | 60 | 74.4 | 25.6 |

*4.3.1.1 Effect of carbonization times*

The carbonization process is the process to increase the carbon content and to create an initial porosity in the char (Li *et al.*, 2008). One of the significant parameter of carbonization process is time. From Table 4.4, under constant temperature at 400°C (size 4-6 mesh, $N_2$ flow rate 150 ml/min), the char yields decreased from 30.2% to 27.8% and burn-off increased from 69.8% to 72.2% with the increasing of carbonization time.

The yields at higher carbonization time of carbonized coconut chars were higher than chars produced at lower carbonization time. Figure 4.25 shows the yield (%) and burn-off (%) vs. time (min) of carbonized char at 400°C. The decreasing in yield was from decomposition of volatiles, cellulose in the temperature ranges of 300-430°C, lignin in the temperature ranges of 250-550°C, and hemicelluloses were decomposes at lower temperature than cellulose and lignin (Hayashi *et al.*, 2002). Furthermore, the dehydrating was occurred during carbonization process of coconut shells and then, the ordering process in their structure of residual carbon can be made, and the polymerization reaction was formed (Li *et al.*, 2008).

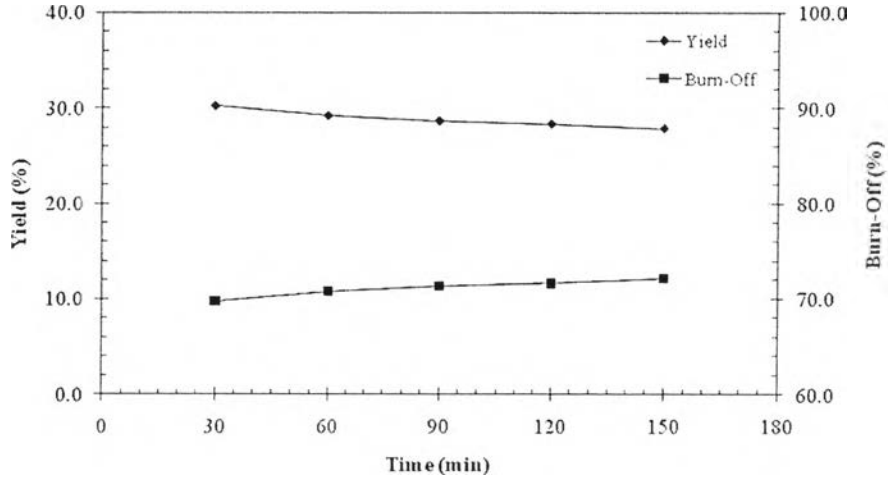


**Figure 4.25** Yield (%) and Burn-off (%) vs. time (min) of carbonized char at 400°C.

*4.3.1.2 Effect of carbonization temperatures*

Table 4.4 and Figure 4.26 present coconut chars prepared under different carbonization temperatures. The yields of chars decreased from 29.2% to 25.6% and burn-off increased from 71.3% to 74.4% with the increasing of carbonization temperatures. The yields decreased while burn-off increased because of the hydrogen, oxygen, and volatiles content were removed from the coconut shell, and solid chars was occurred. The porosity of coconut shell activated carbon was increased to obtain a highly porous material. The higher carbonization temperatures the higher the BET surface area and micropore volume (Daud *et al.*, 2000).

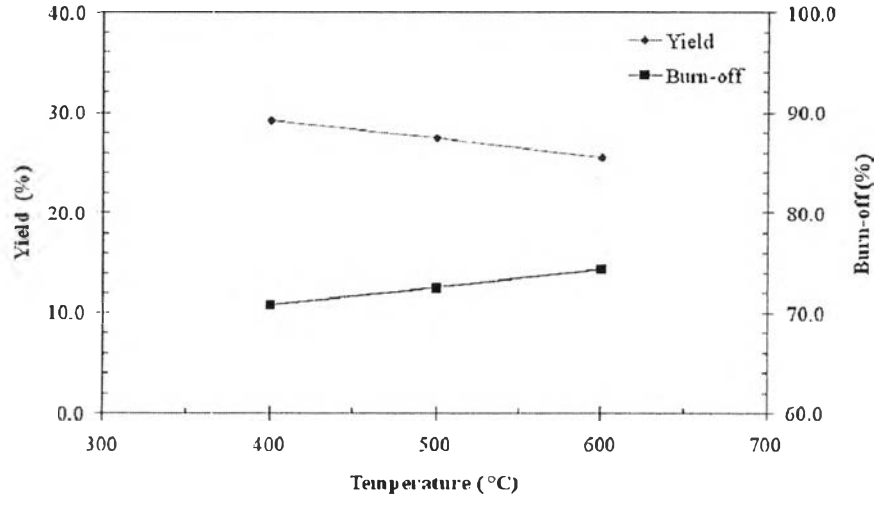


**Figure 4.26** Yield (%) and Burn-off (%) vs. temperature (°C) of carbonized char at 60min.

4.3.2 Activation process (Chemical activation process)

The coconut char (400 °C, 60 min, BET surface area 95.3 $m^2/g$) was impregnated with potassium carbonate solution with ratio 1:1 by weight. The coconut char was heated up with the rate of 10 °C/min, nitrogen flow rate of 100 ml/min to a desired temperature at 600 °C with different periods of time. The carbon product was washed with DI water until pH ≈ 7. The results are shown in Table 4.5.

**Table 4.5** Characteristics of coconut-based activated carbon at different activation conditions

| Sample | Activating agent | $N_2$ flow rate (ml/min) | Temperature (°C) | Time (min) | Burn-off (%) | Yield (%) |
|---|---|---|---|---|---|---|
| Co-$K_2CO_3$/1h | $K_2CO_3$ | 100 | 600 | 60 | 23.6 | 76.4 |
| Co-$K_2CO_3$/2h | $K_2CO_3$ | | | 120 | 24.5 | 75.5 |
| Co-$K_2CO_3$/3h | $K_2CO_3$ | | | 180 | 25.1 | 74.9 |

There are two stages in chemical activation: (i) the micropore formation which starts with the addition of chemical ($K_2CO_3$) to the coconut chars, and (ii) the pore widening which is the result of the chemical effect inside the opened pores. Pore widening normally begins when there are a number of opened pores in the structure; therefore, it becomes significant when the impregnation ratio was reasonably high (Lozano-Castelló *et al.*, 2001). During the activation, coconut chars were heated up then, mass loss would create voids between carbon matrix, BET surface area increase and carbon in the chars was removed by formation of CO due to the reduction of $K_2CO_3$ follows the equation 4.1 (Hayashi *et al.*, 2002):

$$K_2CO_3 + 2C \rightarrow 2K + 3CO \qquad (4.1)$$

For these reasons, BET surface area, micropore volume, and total pore volume of Co-$K_2CO_3$ at 600°C with increasing activation time of 60 min to 120 min (Figure 4.27-4.28) were increased from 197.9 to 211.3 $m^2/g$, 0.13 to 0.14 cc/g, and 0.14 to 0.16 cc/g, respectively. On the other hand, by increasing activation time from 120 min to 180 min, existing pores in the char structure were enlarged and thus decreasing in BET surface area was observed. This could be the wall of the pores were collapsed by excess activation time. Also, the reduction of micropore volume and total pore volume could be because the ash in the char was melted and blocked the pores at 180 min.

However, using chemical activation would produce highly porous activated carbon but in this study the activated carbon has too low BET surface area, low micropore volume, low total pore volume, and large pore diameter. This was probably because the activation temperature was too low to let the activated carbon became a high porous material. Moreover, the amount of DI water might not be enough to remove the basic and water-soluble components from activated carbon, thus the pores of activated carbon were blocked by the remaining $K_2CO_3$.

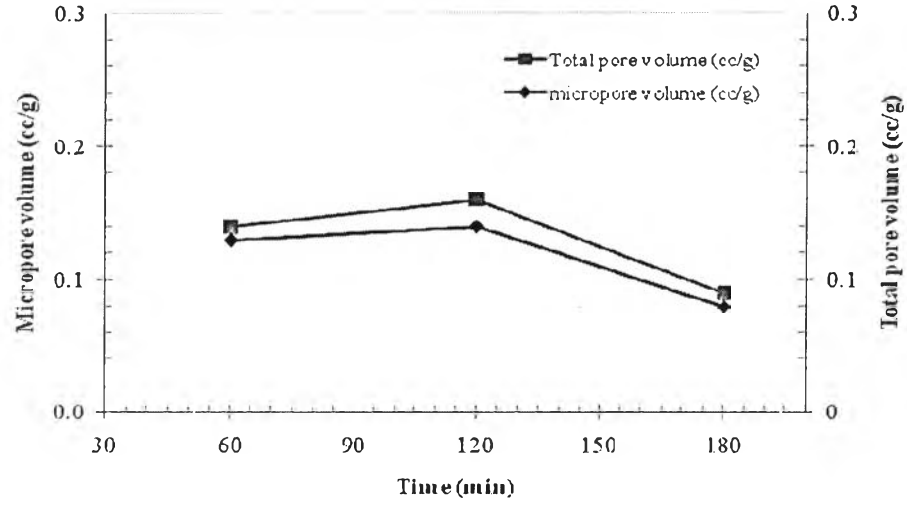


**Figure 4.27** Influence of activation time on the micropore volume (cc/g) and total pore volume of Co-$K_2CO_3$.

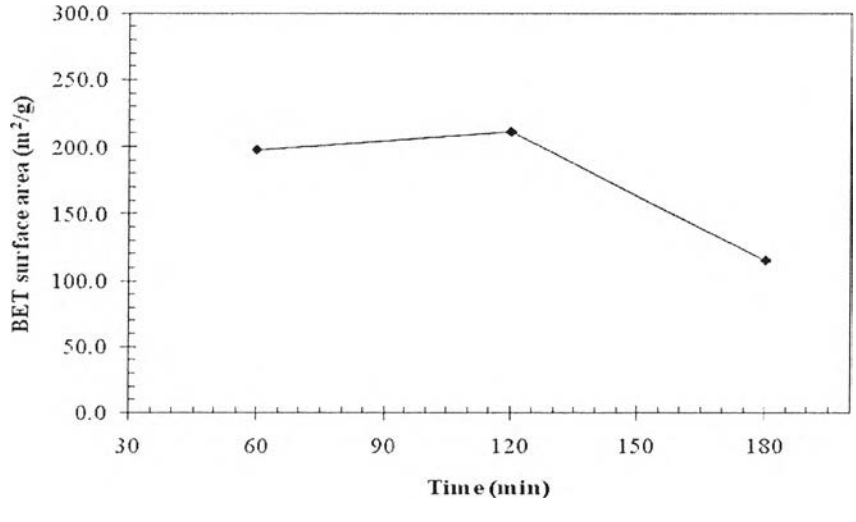


**Figure 4.28** Influence of activation time on the BET surface area ($m^2/g$) of Co-$K_2CO_3$.

Co-$K_2CO_3$ yields were decreased from 76.4% to 74.9% and burn-off increased from 23.6% to 25.1% with increasing of activation time as illustrated in Table 4.5.